Nanoscience and Nanotechnology 2018, 8(2): 25-30
DOI: 10.5923/j.nn.20180802.01

Serum Albumin Protein-Mediated Ultra-Fast Laser Synthesis of Calcium Phosphate Nanoceramic in Aqueous Solution

Marina Rodio[1,2], Romuald Intartaglia[3,*]

[1]Hamburg Centre for Ultrafast Imaging, Luruper Chaussee 149, Hamburg, Germany
[2]Physical Chemistry, Hamburg University, Martin-Luther-King Platz 6, Hamburg, Germany
[3]Nanophysics, Istituto Italiano di Tecnologia, Via Morego 30, Genoa, Italy

Abstract Ceramic nanoparticles are promising biomaterials for bone tissue regeneration, cell proliferation and as plasmid DNA delivery vector, because they bear outstanding properties of chemical similarity to the human mineral constituent, bioactivity, and are fairly easily bio-conjugated. Here we report on the synthesis of hydroxyapatite nanoparticles by laser ablation of hydroxyapatite target in deionized water and in aqueous solution of Serum Albumin protein. Laser ablation in deionized water results in the formation of large clusters composed by small nanoparticles, while in Serum Albumin protein solution a starting process of clusters disaggregation is observed. Stability and nanoparticle size-quenching effect is investigated by various methods such as electron microscopy zeta potential and dynamic light scattering. It is found that the presence of Serum Albumin protein in aqueous solution plays the role of size-regulating agent. The integrity of Serum Albumin protein after laser irradiation is assessed by means of UV-vis and FT- IR analysis. Further, the chemical structure and crystallinity of the hydroxyapatite colloidal solution is investigated by infrared spectroscopy, X-Ray diffraction measurement and energy-dispersive X-ray diffraction.

Keywords Calcium phosphate, Hydroxyapatite, Serum Albumin Protein, Laser Synthesis in Liquid, Green synthesis

1. Introduction

Hydroxyapatite nanoparticles (HA-NPs) are promising biomaterials due to their outstanding properties[1] of biocompatibility, biodegrability, bioactivity, and chemical and structural similarity to the human mineral constituent, leading to applications in the tissue engineering field [2], medical implants [3, 4], cell proliferation [5, 6] and in-vivo delivery of biomolecules (plasmid DNA [7, 8] or Protein [9]). HA-based nanostructures with size less than 100 nm exhibits enhanced resorbability [10] and bioactivity [5, 11], osteogenic activity [12-14], osteoblast adhesion [12] as well as a promotion of cell growth and inhibition of cell apoptosis [15], with respect to larger or micro-sized hydroxyapatite [16]. Various methods have been developed to prepare HA based nanoparticles such as dry methods [17], high temperature processes [18] and wet chemical methods [19-21]. The wet chemical methods are attractive because size and surface properties can be controlled at once. However this method involves the use of salts precursors and/or reducing agents [22] which can interfere with subsequent stabilization during the functionalization step or require multi-step procedures, i.e., long term aging and heat treatment steps. [23] Swain et al. reported crystalline hydroxyapatite nanoparticles with 60 nm mean size by co-precipitation technique combined with heat treatment in the range from 700°C to 1250°C. [24] Other groups obtained hydroxyapatite nanoparticles with a size around 100 nm by sol-gel approach and heat treatment steps (800°C), with crystallinity but different phases [23, 25]. Nowadays, Pulsed Laser Ablation in Liquid (PLAL) has gained a great deal of attention for simplicity of the procedure, which lets the synthesis of a wide range of nanoparticles, i.e., metallic [26-28], semiconductor [29-31], and ceramic [32]. Compared to chemical synthesis, PLAL technique appears to be the most flexible and promising technique, because of its many advantages for biomedical applications. (i) PLAL does not necessarily require any chemicals and does not necessarily produce waste: it is defined "green" method [33]; (ii) one step functionalization is easy, since the functional molecules can be simply added to the colloidal solution [34-36]; (iii) PLAL technique allows the production of NPs on the gram scale per hour

* Corresponding author:
romuald.intartaglia@iit.it (Romuald Intartaglia)
Published online at http://journal.sapub.org/nn

[37]. In this work, we report on the formation of hydroxyapatite nanoparticles by ultra-fast laser ablation of hydroxyapatite target in deionized water and in aqueous solution of biomolecule. Laser ablation in deionized water results in the formation of large clusters of micrometers in size, i.e., ~700 nm, composed by small nanoparticles while in biomolecules solution a starting process of clusters disaggregation is observed leading to the formation of nanoparticles with a mean size of ~ 90 nm. Electron microscopy, dynamic light scattering and zeta potential measurements were performed, indicating that the presence of biomolecules in aqueous solution plays the role of stabilizing agents for HA-NPs. Further, the chemistry, crystallinity and chemical structure of the obtained colloidal solution is investigated by infrared spectroscopy, X-ray and Energy-dispersive diffraction.

2. Materials and Methods

2.1. Laser Synthesis of Hydroxyapatite Nanoparticles in Aqueous Solution

Hydroxyapatite nanoparticles (HA-NPs) have been prepared by ultra-short laser ablation of hydroxyapatite bulk (HA) in deionized water and in aqueous solution of protein. Bovine Serum Albumin (BSA) protein is added to deionized water before the ablation at a concentration of 10^{-9} M. For each sample, the target was irradiated for 10 min at a fluency of 4 J cm^{-2}. Laser ablation experiments were carried out using a picosecond Nd:YAG laser (continuum leopard) providing a pulse centered at 1064 nm with a maximum pulse energy of 115 mJ at a repetition rate of 20 Hz. The laser pulse energy was controlled with a variable attenuator. The laser beam was focused 1 cm below the target surface using a lens with a focal length of 25 cm. The hydroxyapatite target (CELLYARDTM pellet, PENTAX), in the form of a disc with a diameter of 5 mm and a thickness of 2 mm, was placed on the bottom of a quartz cuvette and immersed in 1 mL of solution. Before each experiment the target was washed with deionized water several times to remove the impurity from the surface. During laser ablation, the target was moved with a rotation system (T-cube DC Servo controller, Thor labs) to achieve uniform irradiation of the surface. Figure 1 shows a schematic of ultra-fast laser ablation of hydroxyapatite target placed in aqueous solution.

2.2. Characterisation

Conventional Transmission Electron Microscopy (TEM) was performed with a JEOL Jem1011 microscope working at an acceleration voltage of 100 kV. Conventional TEM samples were prepared by dropping the colloidal solution directly onto a carbon-coated 300 mesh copper grids and allowing the aqueous solution to evaporate under room temperature and pressure.

Energy-Dispersive X-Ray spectroscopy (EDX) characterization was performed on a High Resolution Scanning Electron Microscope (HRSEM) Jeol JSM-7500F equipped with a cold field emission gun using an Oxford X-Max 80 system with a silicon drift detector (SDD) having an 80 mm2 effective area. The analyses were done with an accelerating voltage of 10 kV and the spectra were acquired for 600 s live time. Standardless quantification was achieved with Aztec Energy EDX Software.

X-Ray Diffraction (XRD) spectra were recorded using a Smartlab 9kW Rigaku diffractometer equipped with a copper rotating anode. The X-ray source was operated at 40kV and 150 mA. A Göbel mirror was used to obtain a parallel beam and to suppress Cu Kβ radiation (1.392 Å). The 2 theta/omega scan was performed with two radiations, Cu Kα1 (1.544 Å) and Cu Kα2 (1.541 Å), with a step of 0.05° (2theta). Specimens were prepared by drop-casting a solution of HA-NPs onto zero-background silicon wafers. The software PDXL by Rigaku was used for qualitative analysis.

The morphology and zeta potential analysis of the laser-synthesized HA-NPs in deionized water and in BSA protein aqueous solution were performed using a Zetasizer Nano ZS (Malvern Instruments). Each solution was injected into disposal quartz cuvette for the evaluation of particles mean hydrodynamic size and into semi-micro disposable quartz electrophoretic cell for the stability evaluation. The Smoluchowski model was used to calculate the zeta potential value. All data represent the average of triplicate measurements of the samples prepared in three different procedures.

Optical absorption spectra were recorded in quartz cuvette using a Cary 6000 UV-VIS-NIR double beam spectrophotometer. Fourier Transform Infrared (FT-IR) spectroscopy analysis were performed using the Bruker Vertex 80V infrared spectrometer in the range (600-4000) cm^{-1}. Samples were prepared by drop-casting centrifuged solutions of HA-NPs on a CaF_2 substrate and by drying them overnight in vacuum chamber.

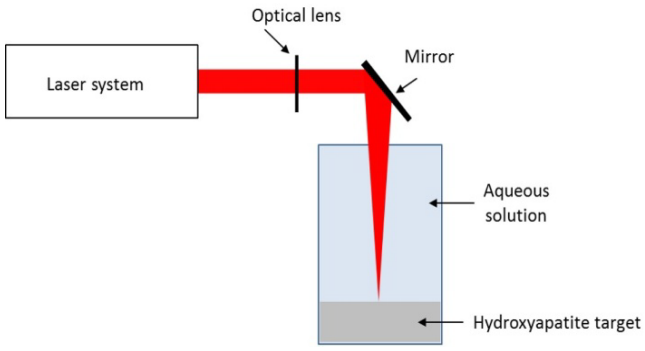

Figure 1. Schematic of ultra-fast laser ablation of hydroxyapatite target placed in aqueous solution

3. Results and Discussions

HA-NPs colloidal solution were prepared by ultra-fast laser ablation of HA target in deionized water. Figure 2a

shows the as-synthesized HA-NPs in water displaying the formation of HA aggregates of micrometers in size with a not well defined shape. The formed HA clusters are composed of small HA-NPs with size less than 50 nm, as shown in Figure 2b. The formation mechanism starts a few tens of picoseconds after the laser ablation and the plasma lasts for tens of nanoseconds. In the case of the ablation with nanosecond pulses, there is temporal overlap between the pulses and the laser-generated plasma, i.e., the ejected material and the heating related ablation can also occur in a region larger than the irradiated area. This temporal overlap produces an expanding plume composed by a mixture of ionized atoms, clusters and larger fragments, leading to the formation of large HA-NPs. [32] On the contrary, in the case of laser ablation with ultra-fast laser pulses, i.e., picosecond, there is no temporal overlap with the ablated material; the plasma evolves without any other heating, and radiation process resulting in the formation of small HA-NPs. Since the temperature in the laser-generated plasma is locally high (thousands of Kelvin), the nucleation and crystallization occur simultaneously allowing the formation of NPs nanostructures, while their agglomeration is the result of the low stability of the unconjugated HA-NPs, as shown in Figure 4.

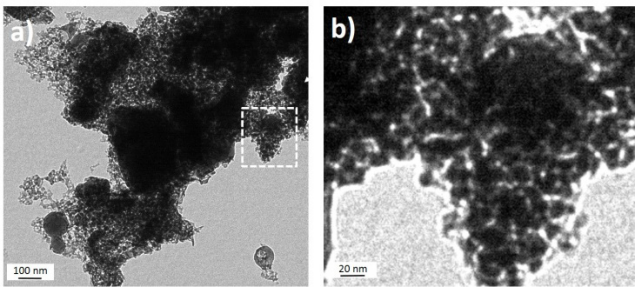

Figure 2. a) TEM image of HA-NPs solution obtained by infrared picosecond laser ablation of HA target in deionized water. b) TEM magnification of the selected area, i.e., white dashed line

In comparison with the HA colloidal solution prepared in deionized water, the one prepared in BSA solution shows a starting process of clusters disaggregation. Figure 3 shows TEM images of HA-NPs produced by ultrafast laser ablation of HA target in 10^{-9} M BSA protein aqueous solution, at different magnification, scale bars a) 100 nm b) 50 nm c) 20 nm. Of note, we can observe the presence of large cluster together with isolated HA nanoparticles. (Figure 3a) The size distribution of the nanoparticles represented in the electron microscopy images is shown in Figure 3d. The statistical analysis reveals a mean size value of (90 ± 30) nm. We can conclude that the presence of biomolecules in the aqueous solution protein influences the aggregation state and thus the nanoparticles size during the laser processing.

The starting process of clusters disaggregation is investigated by dynamic light scattering and zeta potential measurements. Figure 4 shows the hydrodynamic diameter (a) and zeta potential values (b) of the colloidal solution prepared in deionized water and in aqueous solution of BSA. The hydrodynamic diameter of the HA colloidal solution prepared in deionized water is around (700 ± 150) nm, while the one prepared in aqueous solution of BSA has a value around (440 ± 60) nm. This size reduction effect is in agreement with a disaggregation phenomena of the clusters in smaller one, as discussed above. Moreover, the obtained value of zeta potential confirms the observed trend. The zeta potential value of the colloidal solution prepared in deionized water is (-10.0 ± 5.0) mV, while the one prepared in aqueous solution of BSA has a value around (-20.7 ± 7.5) mV. The low zeta potential of the colloidal solution prepared in deionized water is in agreement with the TEM analysis (Figure 2) showing the presence of large clusters of micro-meter in size composed by small nanoparticles.

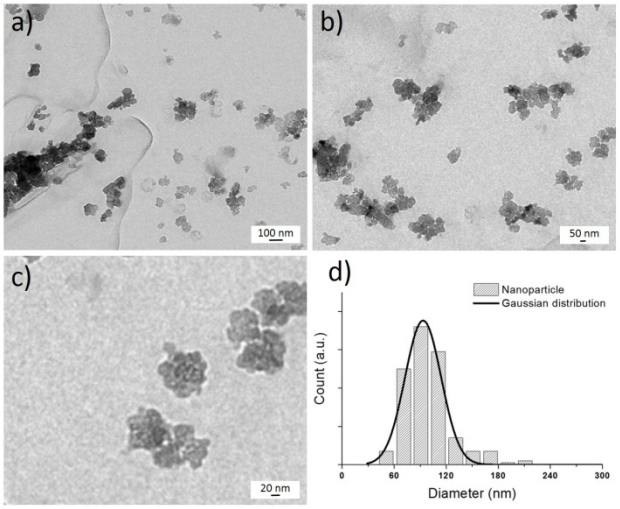

Figure 3. a) TEM images of HA-NPs produced by ultrafast laser ablation of HA target in 10^{-9} M BSA protein aqueous solution, at different magnification, scale bars a) 100 nm b) 50 nm c) 20 nm and d) NPs size distribution

During the laser processing in deionized water, nanoparticles with low stability are formed and then aggregated to form large clusters. The variation of the zeta potential of the colloidal solution prepared in aqueous solution of biomolecules towards lower negative value is also in agreement with the disaggregation state of the clusters. We can conclude that the presence of BSA molecules in aqueous solution plays the role of stabilizing agent for HA-NPs during the laser process.

Structural and compositional analysis by X-Ray Diffraction (XRD) and Energy-dispersive X-ray (EDX) spectroscopy, respectively, were been performed on the HA-NPs colloidal solution prepared in 10^{-9} M BSA protein aqueous solution. XRD analysis (Figure 5a) confirms the crystallinity of the HA-NPs displaying index of Miller typical of the hexagonal structure $Ca_{10}(PO_4)_6(OH)_2$ in P63m space group (JSPDS No. 09-0432). The EDX spectrum of the synthesized HA-NPs colloidal solution is reported in Figure 5b.

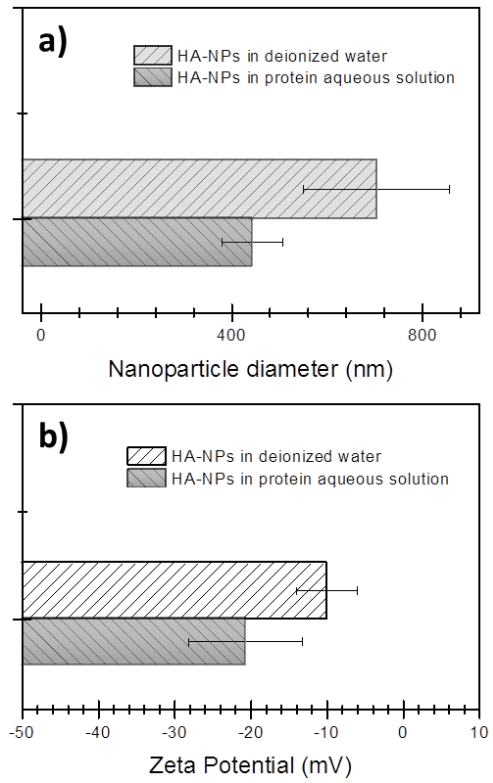

Figure 4. a) Hydrodynamic size and b) zeta potential values of HA colloidal solutions obtained by picosecond laser ablation of hydroxyapatite target placed in deionized water, and 10^{-9} M BSA protein aqueous solution

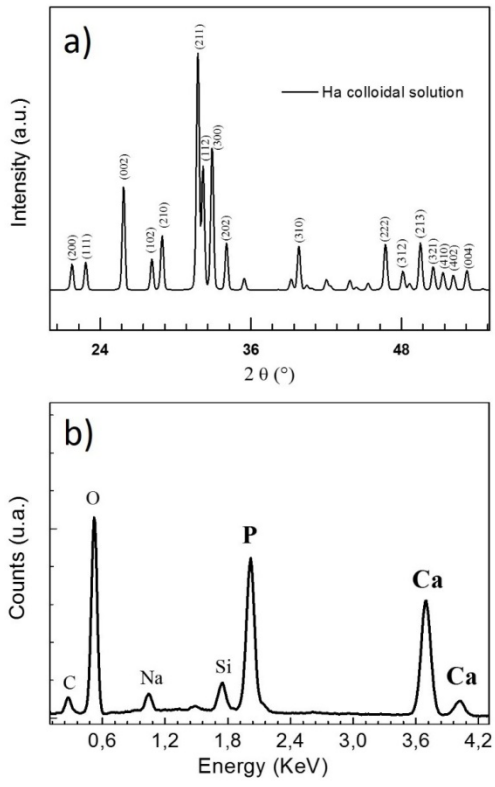

Figure 5. a) X-Ray and b) Energy-dispersive X-ray diffraction profiles of HA-NPs prepared by ultra-fast laser ablation of HA target in BSA solution. Peaks corresponding to the Phosphate (P) and Calcium (Ca) elements of HA-NPs are observed

Peaks corresponding to the Phosphate (P) and Calcium (Ca) elements of HA-NPs are observed. The other peaks, Si, Na, and C comes from Silicon substrate, deionized water and air contaminations, respectively. Standardless chemical quantification was achieved with Aztec Energy EDX Software, providing a Ca/P stoichiometric ratio value near to 1.65 ± 0.02, in agreement with HA bulk. These results indicate that the structural properties of the HA bulk are preserved during the synthesis of HA-NPs by laser ablation in liquid process.

The integrity of serum albumin protein during laser process were investigated by absorption and infrared spectroscopy. Figure 6 shows the absorption spectra of fresh BSA solution and HA-NPs laser-synthesized in serum albumin protein solution. We observed that the peak intensity of BSA and HA colloid solution in BSA after ablation was found to be nearly the same, i.e., 280 nm indicating a high degree of molecule integrity. [33]

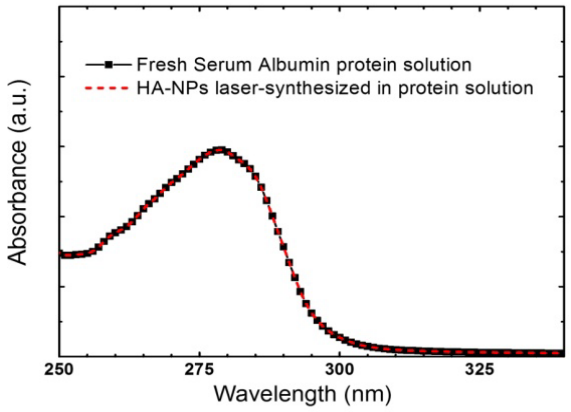

Figure 6. Absorption spectra of fresh Serum Albumin protein (black line), i.e., before laser process, and HA-NPs colloid solution prepared in Serum Albumin protein aqueous solution (red dashed line), i.e., after laser process

Figure 7 shows the FT-IR spectrum in the range (700-3700) cm^{-1} of laser-synthesized HA-NPs in 10^{-9} M BSA aqueous solution. First, it shows all the typical peaks of HA reported in literature [38]. The most intense peaks at 1047 cm^{-1} and the 1090 cm^{-1}, correspond to ν3 phosphate mode. The peak at 960 cm^{-1} corresponds to ν1 phosphate mode. The band at 3300 cm^{-1} may come from lattice H2O because this band exists in the range of (3200–3550) cm^{-1}. [38] The other peaks present in the spectrum correspond to typical Serum Albumin protein peaks. [39] The stretching band at 1658 cm^{-1} and 1540 cm^{-1} are assigned to the stretching and bending vibration in protein amide-I (α helix structure) and amide–II (β sheet structure), respectively. Of note, the observation of these bands indicates that the physical structure of protein is preserved during laser ablation process. Aggregation and denaturation of the protein induced by external factors are usually characterized by a position shift of secondary structure band (Amide I and Amide II). [40] The 3300 cm^{-1} and 2960 cm^{-1} bands represent the N-H vibrational mode, and -CH stretching mode of the Serum Albumin protein, respectively. The

stretching mode of the group (COO) is identified by the band at 1399 cm^{-1}. [39]

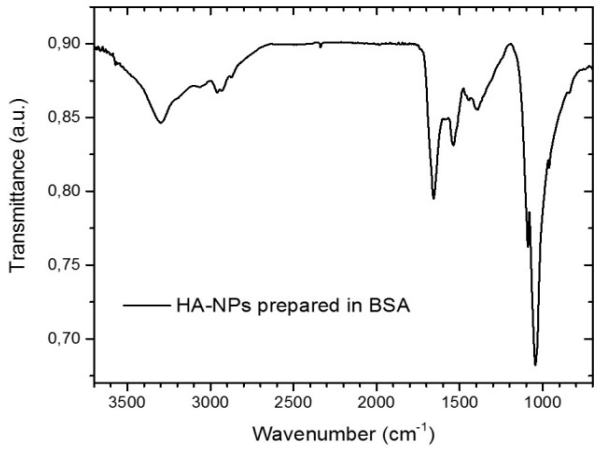

Figure 7. FT-IR spectra of HA-NPs colloidal solution synthesized in 10^{-9} M BSA protein aqueous solution

4. Conclusions

We have reported on the synthesis and characterization of hydroxyapatite nanoparticles via ultra-fast laser ablation of hydroxyapatite target placed in deionized water and in aqueous solution of Serum Albumin protein. Electron microscopy, dynamic light scattering and zeta potential analysis showed that the synthesized HA-NPs in protein aqueous solution displayed HA nanoparticles with smaller size and less agglomerated compared to HA synthesized in deionized water. The Serum Albumin protein in solution acts as an in-situ size-regulating agent. Infrared spectroscopy, X-ray and Energy-dispersive diffraction indicated similar chemical and compositional structure to hydroxyapatite ceramic bulk, while the protein integrity after the laser irradiation was assessed by optical spectroscopy. Our synthesis approach overcomes conventional solution routes by avoiding the use of hazardous organic and/or unhealthy organic solvents and temperature treatments. Further advantages of being inexpensive, clean and easily scalable for biomaterials industry, open exciting possibilities to generate a wide range of HA-NPs, promising as versatile bioactive tool for in-vivo applications.

ACKNOWLEDGEMENTS

The authors acknowledge Hamburg Centre for Ultrafast Imaging and Istituto Italiano di Tecnologia for financial support.

REFERENCES

[1] Surmenev, R.A., M.A. Surmeneva, and A.A. Ivanova, *Significance of calcium phosphate coatings for the enhancement of new bone osteogenesis – A review.* Acta Biomaterialia, 2014. 10(2): p. 557-579.

[2] Zhou, H. and J. Lee, *Nanoscale hydroxyapatite particles for bone tissue engineering.* Acta Biomaterialia, 2011. 7(7): p. 2769-2781.

[3] Baino, F., et al., *Biomaterials for orbital implants and ocular prostheses: Overview and future prospects.* Acta Biomaterialia, 2014. 10(3): p. 1064-1087.

[4] Farkas, B., et al., *Fabrication of hybrid nanocomposite scaffolds by incorporating ligand-free hydroxyapatite nanoparticles into biodegradable polymer scaffolds and release studies.* Beilstein J Nanotechnol, 2015. 6: p. 2217-23.

[5] Cai, Y., et al., *Role of hydroxyapatite nanoparticle size in bone cell proliferation.* Journal of Materials Chemistry, 2007. 17(36): p. 3780-3787.

[6] Cai, L., A.S. Guinn, and S. Wang, *Exposed hydroxyapatite particles on the surface of photo-crosslinked nanocomposites for promoting MC3T3 cell proliferation and differentiation.* Acta Biomater, 2011. 7(5): p. 2185-99.

[7] Choi, S. and W.L. Murphy, *Sustained plasmid DNA release from dissolving mineral coatings.* Acta Biomater, 2010. 6(9): p. 3426-35.

[8] Mostaghaci, B., et al., *One-Step Synthesis of Nanosized and Stable Amino-Functionalized Calcium Phosphate Particles for DNA Transfection.* Chemistry of Materials, 2013. 25(18): p. 3667-3674.

[9] Combes, C. and C. Rey, *Adsorption of proteins and calcium phosphate materials bioactivity.* Biomaterials, 2002. 23(13): p. 2817-2823.

[10] Motskin, M., et al., *Hydroxyapatite nano and microparticles: Correlation of particle properties with cytotoxicity and biostability.* Biomaterials, 2009. 30(19): p. 3307-3317.

[11] Dong, Z., Y. Li, and Q. Zou, *Degradation and biocompatibility of porous nano-hydroxyapatite/ polyurethane composite scaffold for bone tissue engineering.* Applied Surface Science, 2009. 255(12): p. 6087-6091.

[12] Lin, K., et al., *Tailoring the Nanostructured Surfaces of Hydroxyapatite Bioceramics to Promote Protein Adsorption, Osteoblast Growth, and Osteogenic Differentiation.* ACS Applied Materials & Interfaces, 2013. 5(16): p. 8008-8017.

[13] Sadat-Shojai, M., et al., *Nano-hydroxyapatite reinforced polyhydroxybutyrate composites: A comprehensive study on the structural and in vitro biological properties.* Materials Science and Engineering: C, 2013. 33(5): p. 2776-2787.

[14] Rodio, M., et al., *Facile fabrication of bioactive ultra-small protein–hydroxyapatite nanoconjugates via liquid-phase laser ablation and their enhanced osteogenic differentiation activity.* Journal of Materials Chemistry B, 2017. 5(2): p. 279-288.

[15] Shi, Z., et al., *Size effect of hydroxyapatite nanoparticles on proliferation and apoptosis of osteoblast-like cells.* Acta Biomaterialia, 2009. 5(1): p. 338-345.

[16] Bose, S., et al., *Microwave-processed nanocrystalline hydroxyapatite: Simultaneous enhancement of mechanical and biological properties.* Acta Biomaterialia, 2010. 6(9): p. 3782-3790.

[17] Yeon, K.C., J. Wang, and S.C. Ng, *Mechanochemical synthesis of nanocrystalline hydroxyapatite from CaO and CaHPO4.* Biomaterials, 2001. 22(20): p. 2705-12.

[18] Tas, A.C., *Combustion synthesis of calcium phosphate bioceramic powders.* Journal of the European Ceramic Society, 2000. 20(14–15): p. 2389-2394.

[19] Dhand, V., K.Y. Rhee, and S.-J. Park, *The facile and low temperature synthesis of nanophase hydroxyapatite crystals using wet chemistry.* Materials Science and Engineering: C, 2014. 36(0): p. 152-159.

[20] Ma, M.G., *Hierarchically nanostructured hydroxyapatite: hydrothermal synthesis, morphology control, growth mechanism, and biological activity.* Int J Nanomedicine, 2012. 7: p. 1781-91.

[21] Bakan, F., O. Laçin, and H. Sarac, *A novel low temperature sol-gel synthesis process for thermally stable nano crystalline hydroxyapatite.* Powder Technology, 2013. 233: p. 295-302.

[22] Viswanath, B. and N. Ravishankar, *Controlled synthesis of plate-shaped hydroxyapatite and implications for the morphology of the apatite phase in bone.* Biomaterials, 2008. 29(36): p. 4855-63.

[23] Sanosh, K.P., et al., *Preparation and characterization of nano-hydroxyapatite powder using sol-gel technique.* Bulletin of Materials Science, 2009. 32(5): p. 465-470.

[24] Swain, S.K. and D. Sarkar, *A comparative study: Hydroxyapatite spherical nanopowders and elongated nanorods.* Ceramics International, 2011. 37(7): p. 2927-2930.

[25] Iafisco, M., et al., *Conjugation of hydroxyapatite nanocrystals with human immunoglobulin G for nanomedical applications.* Colloids and Surfaces B: Biointerfaces, 2012. 90(0): p. 1-7.

[26] Intartaglia, R., et al., *Extensive characterization of oxide-coated colloidal gold nanoparticles synthesized by laser ablation in liquid.* Materials, 2016. 9(9): p. 775.

[27] Kőrösi, L., et al., *Ultrasmall, ligand-free Ag nanoparticles with high antibacterial activity prepared by pulsed laser ablation in liquid.* Journal of Chemistry, 2016. 2016.

[28] García-Calzada, R., et al., *Facile laser-assisted synthesis of inorganic nanoparticles covered by a carbon shell with tunable luminescence.* RSC Advances, 2015. 5(62): p. 50604-50610.

[29] Intartaglia, R., et al., *Optical Properties of Femtosecond Laser-Synthesized Silicon Nanoparticles in Deionized Water.* The Journal of Physical Chemistry C, 2011. 115(12): p. 5102-5107.

[30] Intartaglia, R., et al., *Luminescent silicon nanoparticles prepared by ultra short pulsed laser ablation in liquid for imaging applications.* Opt. Mater. Express, 2012. 2(5): p. 510-518.

[31] Rodio, M., et al., *Tailoring of size, emission and surface chemistry of germanium nanoparticles via liquid-phase picosecond laser ablation.* Journal of Materials Chemistry C, 2017. 5(46): p. 12264-12271.

[32] Musaev, O.R., et al., *Nanoparticle fabrication of hydroxyapatite by laser ablation in water.* Journal of Applied Physics, 2008. 104(8): 63.

[33] Intartaglia, R., et al., *Bioconjugated silicon quantum dots from one-step green synthesis.* Nanoscale, 2012. 4(4): p. 1271-1274.

[34] Bagga, K., et al., *Laser-assisted synthesis of Staphylococcus aureus protein-capped silicon quantum dots as bio-functional nanoprobes.* Laser Physics Letters, 2013. 10(6).

[35] Rodio, M., et al., *Direct surface modification of ligand-free silicon quantum dots prepared by femtosecond laser ablation in deionized water.* J Colloid Interface Sci, 2016. 465: p. 242-8.

[36] Papadopoulou, E.L., et al., *Nanocomposite fabrication via direct ultra-fast laser ablation of titanium in aqueous monomer solution.* Laser Physics Letters, 2015. 12(12): p. 125601.

[37] Intartaglia, R., K. Bagga, and F. Brandi, *Study on the productivity of silicon nanoparticles by picosecond laser ablation in water: towards gram per hour yield.* Optics Express, 2014. 22(3): p. 3117-3127.

[38] Han, Y., X. Wang, and S. Li, *A simple route to prepare stable hydroxyapatite nanoparticles suspension.* Journal of Nanoparticle Research, 2009. 11(5): p. 1235-1240.

[39] Grdadolnik, J. and Y. Marechal, *Bovine serum albumin observed by infrared spectrometry. II. Hydration mechanisms and interaction configurations of embedded H(2)O molecules.* Biopolymers, 2001. 62(1): p. 54-67.

[40] Bouhekka, A. and T. Bürgi, *In situ ATR-IR spectroscopy study of adsorbed protein: Visible light denaturation of bovine serum albumin on TiO2.* Applied Surface Science, 2012. 261(0): p. 369-374.